Elucidating the initial oxidation of Pt(111) using large-scale atomistic thermodynamics: a ReaxFF Study

Boden, D.; Groot, I.M.N.; Meyer, J.

THE JOURNAL OF PHYSICAL CHEMISTRY C
A JOURNAL OF THE AMERICAN CHEMICAL SOCIETY

pubs.acs.org/JPCC

Article

Elucidating the Initial Oxidation of Pt(111) Using Large-Scale Atomistic Thermodynamics: A ReaxFF Study

Dajo Boden,* Irene M. N. Groot, and Jörg Meyer*

Cite This: *J. Phys. Chem. C* 2022, 126, 20020−20027

Read Online

ACCESS | Metrics & More | Article Recommendations | Supporting Information

ABSTRACT: *In situ* scanning tunneling microscopy experiments on the initial oxidation of Pt(111) found complex intermediary platinum surface oxides, consisting of spoke wheel and stripe structures [*Nat. Commun.***2017**, *8*, 429]. While the stripes have been investigated extensively in the following, the spoke wheels are poorly understood because of their size and complexity. Here we employ atomistic thermodynamics based on an established reactive force field to investigate the structure and stability of spoke wheels at the elevated temperature (>530 K) and pressure (1−4 bar) conditions of the *in situ* experiments. At those conditions, the thermodynamic stability of the structural model for the spoke wheel is similar to that of the stripes, while the degree of surface oxidation is much lower. The spoke wheel is found to be much more stable than partially formed stripes with a similar degree of oxidation. These results are consistent with experimental findings, where the spoke wheel is observed first, at slightly lower oxygen pressures. They thus provide a better understanding of the oxidation pathway for Pt(111)-based catalysts in the context of oxidative catalysis.

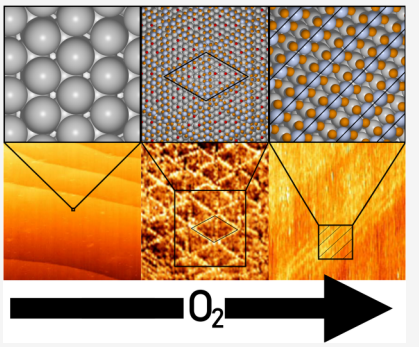

1. INTRODUCTION

Platinum is one of the most important metals in heterogeneous catalysis due to its widespread use in the automotive industry.[1] Platinum is vital for the functioning of the so-called three-way catalyst, which aims to reduce hazardous emissions in cars by reducing NO_x and oxidizing CO and hydrocarbons to CO_2. To do so effectively, cars frequently utilize "lean" operating conditions, meaning they operate with an excess of oxygen.[1,2] Because of this, the platinum nanoparticles in the three-way car catalyst are regularly exposed to oxygen and other highly oxidative gases at high temperatures (>500 K). Additionally, platinum is used in hydrogen fuel cells as a catalyst for the oxygen reduction reaction (ORR), whereby the presence of surface oxides greatly affects the catalytic activity and stability.[3−5] This means that it is essential to better understand the oxidation behavior of platinum for both current and future applications in catalysis.

Because of its great potential as a catalyst for oxidation reactions, the interaction between platinum and oxygen has been studied extensively for over 100 years, since the very beginning of the field of surface science.[6] To improve the catalyst by means of rational design, its *modus operandi* needs to be understood. The majority of these studies are performed under ultra-high vacuum (UHV) conditions, which is practical because most experimental surface science techniques require a gas-free environment to work.[7−10] Additionally, it allows for an atomically clean and well-characterized catalyst surface, thus giving a greater degree of control over the reaction conditions. In conjunction with these UHV studies, computational tools based on fundamental quantum mechanical principles, such as density functional theory (DFT), are commonly utilized to explain and support experimental findings.[11,12] These computational studies are frequently performed for model systems from UHV studies under low-pressure conditions. An increasing number of *in situ* experiments show, however, that these model systems are often not representative of the surface under catalytic conditions, which is often described as the *pressure gap*.[13,14]

Recent *in situ* scanning tunneling microscopy (STM) studies under conditions realistic for catalysis have shown that the surface of a Pt(111) single crystal partially oxidizes at high temperature (>530 K) and pressure (1−4 bar of O_2).[15] At around 1 bar a spoke wheel-like structure is formed, while at higher oxygen pressure a striped pattern emerges. At the bias voltage used in the aforementioned *in situ* experiments, the tunneling is expected to occur primarily through Pt atoms. On the basis of Pt−Pt distances obtained from STM and electron binding energies observed with X-ray photoelectron spectroscopy (XPS), the observed structures are expected to be surface oxides.[15] The platinum surface oxides disappear at room temperature in UHV after oxygen exposure, clearly implying that they are not (very) stable under the typical surface science

Received: August 11, 2022
Revised: November 4, 2022
Published: November 18, 2022

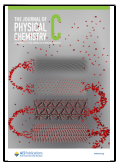

https://doi.org/10.1021/acs.jpcc.2c05769
J. Phys. Chem. C 2022, 126, 20020−20027

conditions. From these findings, it seems clear that the classic surface science approach is not sufficient. To accurately investigate the platinum catalyst, it is important to investigate it at the real conditions of the catalytic process. On the experimental side, this can be achieved by means of *in situ* or *operando* techniques such as in the high-pressure STM employed by van Spronsen et al.,[15] which can provide valuable insights into the mechanism for oxidation and potentially enable extrapolation to the disintegration/corrosion of platinum-based catalysts.

Computationally, atomistic thermodynamics (ATD) is a commonly employed approach to extend atomistic simulations toward finite temperature and pressure conditions.[16−19] By estimating and comparing the relative Gibbs free energy of both bulk and surface structures as a function of temperature and partial pressures, it is possible to construct a full phase diagram of the catalyst from first-principles calculations.[16,20] This technique has recently been used by Hanselman et al.[21] in combination with extensive DFT calculations to determine atomistic models for the stripes and elucidate their role in the oxidation of Pt(111). This study suggests that the stripes seen with STM emerge from a PtO_2-like arrangement, whereby platinum atoms in the stripe rise above the Pt(111) surface. Nevertheless, these findings elucidate only a small part of the complete oxidation process of the Pt(111) surface.

In this work we aim at including the spoke wheels in the understanding of (the initial stages of) this process. The size of the spoke wheel structures makes DFT calculations very challenging. Instead, we employ a reactive force field (ReaxFF) developed and tested specifically for platinum and different platinum oxides in bulk and surface configurations by Fantauzzi et al.[22] ReaxFF generally comes at several order of magnitude lower computationally costs compared to DFT and relies on bond-order-dependent terms to reproduce electronic-structure-dependent chemical properties without considering the electrons explicitly.[22−25] Before applying the Pt−O ReaxFF to the spoke wheel structures, we benchmark this force field against the aforementioned DFT results for PtO_2 stripes of Hanselman et al.[21] Focusing on the temperature and pressure conditions of the *in situ* STM experiments by van Spronsen et al.,[15] we extend this ATD investigation by determining an atomistic model for the spoke wheels and comparing its stability to that of the striped surface oxides. We conclude with a discussion of potential implications for the initial oxidation stages of the Pt(111) surface.

2. METHODS

2.1. Atomistic Thermodynamics. To compare the relative stability of various structures that can result from the exposure of the Pt(111) to oxygen (O_2), this work employs atomistic thermodynamics with the commonly used notation.[16,18,19,26] Briefly, the change in Gibbs free energy per surface area A for the oxidation of a Pt(111) surface is obtained as

$$\Delta\gamma_{Pt_xO_y}(T,p) \approx \frac{1}{A}\left(E_{Pt_xO_y}(x,y) - E^{ref}_{Pt(111)}(x') + (x'-x)E^{bulk}_{Pt} - y\left[\frac{1}{2}E_{O_2^{gas}} + \Delta\mu_O\right]\right) \quad (1)$$

Here $E_{Pt_xO_y}(x,y)$ is the total energy of an oxidized Pt(111) slab with x Pt atoms and y oxygen atoms, $E^{ref}_{Pt(111)}(x')$ is the total energy of a clean Pt(111) slab, E^{bulk}_{Pt} is the energy per Pt atom for bulk (fcc) platinum, and $E_{O_2^{gas}}$ is the total energy of an O_2 molecule in a vacuum. All terms containing temperature and pressure are contained in $\Delta\mu_O$: the change in chemical potential of the oxygen compared to the reference state, which is O_2 in a vacuum at 0 K. Not considering any vibrational contributions to $\Delta\mu_O$ in a first step, this results in

$$\Delta\mu_O(T,p) \approx -\frac{1}{2}k_BT\left\{\ln\left(\left[\frac{2\pi m}{h^2}\right]^{3/2}\right) + \ln\left(\frac{[k_BT]^{5/2}}{p}\right) + \ln\left(\frac{k_BT}{\sigma^{sym}B_O}\right) + \ln(I^{spin})\right\} \quad (2)$$

where m is the molecular mass. The rotational constant (B_O), the symmetry number (σ^{sym}), and the electronic spin degeneracy of the ground state (I^{spin}) of O_2 can be looked up in thermodynamic tables.[27] The Gibbs free energy per surface area for an oxidized Pt(111) slab ($\gamma_{Pt_xO_y}$) as a function of temperature and pressure is then obtained from

$$\gamma_{Pt_xO_y}(T,p) = \gamma_{Pt(111)} + \Delta\gamma_{Pt_xO_y}(T,p) \quad (3)$$

Usually, the influence of the vibrational free energy on the relative stability of the considered surface oxides can be safely neglected.[18] However, Hanselman et al.[21] have shown that the difference in Gibbs free energy between Pt(111) surface oxides is frequently small enough that vibrational contributions to the free energy may affect their relative stability. This is done via a correction term for $\Delta\gamma_{Pt_xO_y}$ containing the vibrational free energy difference

$$\Delta F^{Pt_xO_y}_{vib}(T,\nu_{O-Pt},\nu_{O_2}) = \frac{y}{A}[F_{vib}(T,\nu_{O-Pt}) - F_{vib}(T,\nu_{O_2})] \quad (4)$$

where ν_{O-Pt} and ν_{O_2} are the characteristic vibrational frequencies of oxygen in the surface oxide and gas phase, respectively. Commonly relying on an Einstein model,[28] F_{vib} can then further evaluated according to the statistical mechanics of independent harmonic oscillators

$$F_{vib}(T,\nu) = k_BT\left\{\frac{\hbar\nu}{2k_BT} + \ln\left(1 - \exp\left[\frac{\hbar\nu}{k_BT}\right]\right)\right\} \quad (5)$$

where only a single characteristic frequency has been considered. Unfortunately, the ReaxFF force field is not able to adequately describe the correct vibrational properties of the O−Pt bonds (see the Supporting Information). By choosing the minimum and maximum expected values for ν_{O-Pt} from experiments, it is possible to estimate the range of $\Delta F^{Pt_xO_y}_{vib}$. The lower limit is obtained for $\nu_{O-Pt} = 460\ cm^{-1}$, the characteristic frequency for chemisorbed oxygen adatoms on Pt(111), which is plotted as a red line in Figure 1. The upper limit of $\Delta F^{Pt_xO_y}_{vib}$ is obtained by including all modes found experimentally for platinum surface oxides ($\nu^{(1)}_{O-Pt} = \nu_{O-Pt}$=460 cm^{-1}, $\nu^{(2)}_{O-Pt}$=780 cm^{-1}, and $\nu^{(3)}_{O-Pt}$=1170 cm^{-1} according to Peuckert and Ibach[29]), resulting in

https://doi.org/10.1021/acs.jpcc.2c05769
J. Phys. Chem. C 2022, 126, 20020−20027

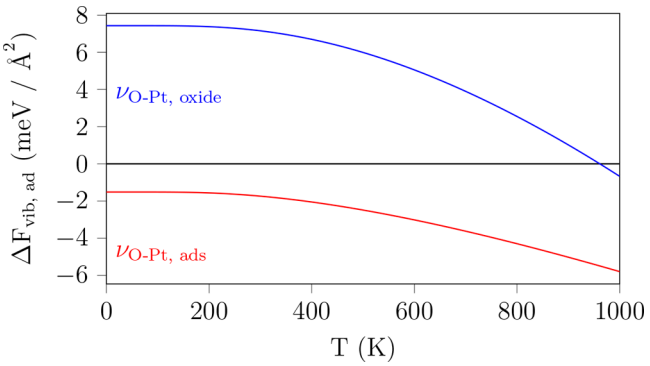

Figure 1. $\Delta F_{vib}^{Pt_xO_y}$ (see eq 4) for a temperature range that is of interest for this work. The red line is for 0.5 ML oxygen adatoms on Pt(111) ($\nu_{O-Pt,ads} = \nu_{O-Pt}$), and the blue line is for platinum surface oxides ($\nu_{O-Pt,oxide} = \{\nu_{O-Pt}^{(1-3)}\}$). See the text for the frequency values.

$$F_{vib}(T, \nu_{O-Pt}^{(1-3)}) = \sum_{i=1}^{3} F_{vib}(T, \nu_{O-Pt}^{(i)}) \tag{6}$$

and plotted as a blue line in Figure 1.

Finally, by considering a large number of different surface configurations explicitly that could be relevant at the experimental conditions this work focuses on (*vide infra* in Section 3.3), we have directly accounted for configurational entropy within the atomistic thermodynamics approach.[18,19]

2.2. Computational Details. All total energies in this work have been calculated with the reactive force field (ReaxFF[22,23]) parametrized for platinum and oxygen by Fantauzzi et al.,[22] using the most recent implementation[30] of ReaxFF[31] in the LAMMPS code (pair_style reaxff).[32] The Atomic Simulation Environment (ASE, ver. 3.22)[33] was used for generating structures and analyzing the output obtained from LAMMPS.

All surface calculations were performed based on a five-layer Pt(111) slab with at least 10 Å vacuum between adjacent periodic images. Because of the cutoff distances included in the Pt−O ReaxFF, increasing the slab thickness or vacuum distance any further has no effect on any of the reported energetics. The default (conjugate gradient) geometry optimizer in LAMMPS has been used for all geometry optimizations, whereby all atoms were allowed to fully relax until the relative change of the total energy; i.e., the change of the total energy between subsequent relaxation steps divided by the absolute value of the total energy is less than 1×10^{-6}. The total energy reference for gas-phase O_2 is obtained for a relaxed O_2 molecule in a cubic box with an edge length 15 Å box.

The relaxed geometries of the PtO_2 stripes as obtained in the DFT calculations by Hanselman et al.[21] have served as starting points (private communications) for a re-relaxation at the ReaxFF level. The exchange-correlation functional according to Perdew, Burke, and Ernzerhof (PBE)[34] has been used in those DFT calculations,[21] which is the same functional that has been used originally for the Pt−O ReaxFF parametrization[22] employed here. Because Fantauzzi et al.[22] had used a different DFT package, the equilibrium lattice constant for bulk platinum deviates slightly from the one obtained by Hanselman et al.[21] (a^{FF} = 3.95 Å vs a^{DFT} = 3.97 Å). Consequently, in this work the starting point PtO_2 stripe structures have been scaled before relaxation (by a factor $\frac{a^{FF}}{a^{DFT}}$) to avoid any artificial stress.

Average oxygen binding energies are calculated according to

$$E_{bind,O} = \frac{1}{n}\left(E_{Pt_mO_n} - E_{Pt(111)_{m'}}^{ref} - (m - m')E_{Pt}^{bulk} - \frac{n}{2}E_{O_2}^{gas}\right) \tag{7}$$

where $E_{Pt_mO_n}$, $E_{Pt}^{ref}(111)_{m'}$, E_{Pt}^{bulk}, and $E_{O_2}^{gas}$ are the total energies obtained from the ReaxFF calculations. The accuracy of these binding energies suffers from the well-known deficiency of the PBE functional (and thus the Pt−O ReaxFF based thereon) to even describe the binding energy of the O_2 molecule in gas phase properly.[35] Consequently, also the Gibbs free energy differences $\Delta\gamma_{Pt_xO_y}$ (see eq 1) are affected. While this can lead to sizable errors for the absolution location of phase boundaries in phase diagrams of oxidized surfaces, this has not been found to change the most stable phases and their relative sequence.[36]

The oxide coverage (θ^{ox}) is defined as

$$\theta^{ox} = \frac{N_O^{PtO_2}}{N_{Pt}^{Pt(111)}} \tag{8}$$

where $N_O^{PtO_2}$ is the number of oxygen atoms coordinated with the lifted Pt atoms and $N_{Pt}^{Pt(111)}$ is the number of Pt atoms in the surface unit cell.

3. RESULTS AND DISCUSSION

3.1. ReaxFF Benchmark for PtO_2 Stripes. The Pt−O ReaxFF that is used in this work has originally been constructed based on different bulk platinum and platinum oxide phases, plus several simple adsorption structures where atomic oxygens reside on different sites of the (otherwise unmodified) Pt(111) surface at different coverages. Those corresponding to the lowest oxygen coverages up to 0.5

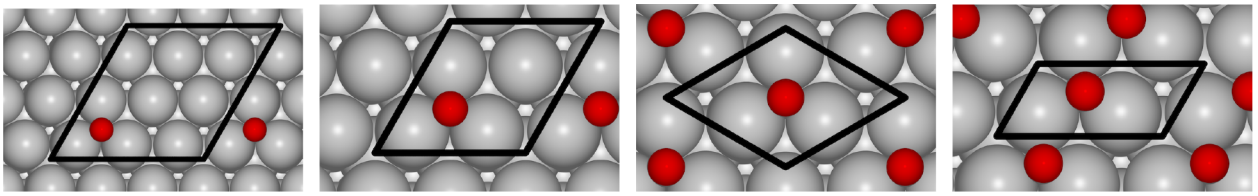

Figure 2. Relaxed structures of the various oxygen adsorption structures. Oxygen atoms are shown in red, while Pt atoms are indicated in gray. The unit cells are indicated in black, and their sizes are given below each panel.

https://doi.org/10.1021/acs.jpcc.2c05769
J. Phys. Chem. C 2022, 126, 20020−20027

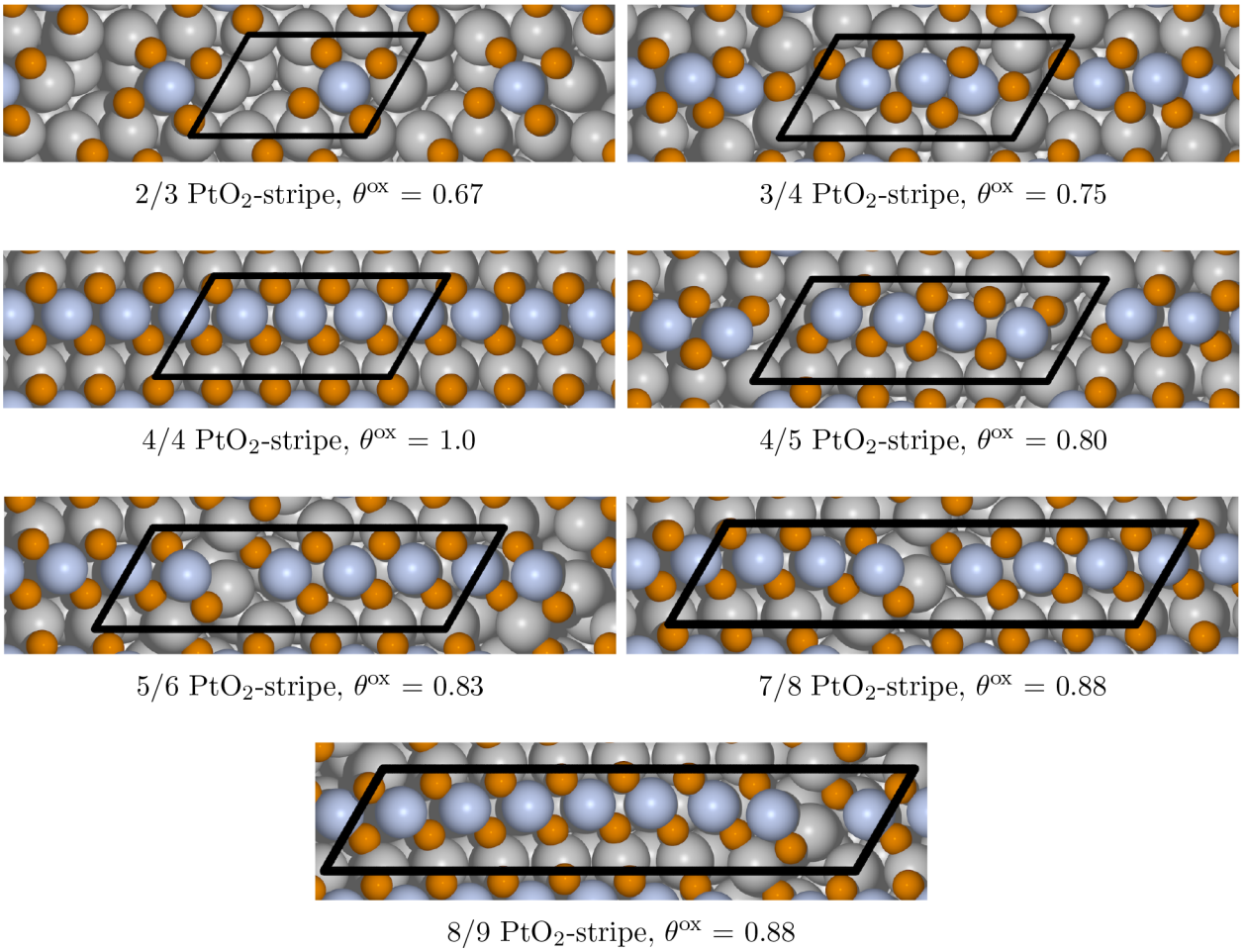

Figure 3. Various platinum surface oxide stripes from Hanselman et al.[21] relaxed using the ReaxFF force field developed by Fantauzzi et al.[22] Oxygen is shown in orange, while metallic and oxidized platinum atoms are indicated in gray and blue, respectively. The unit cells are shown in black.

monolayers (ML) are most relevant in the present context and summarized in Figure 2. To first assess the ability of this ReaxFF force field to describe more complex oxygen adsorption structures including significant reconstruction of the Pt(111) surface, we have benchmarked against the DFT results for the PtO_2 stripes as obtained by Hanselman et al.[21] As shown in Figure 3, all stripe structures remain intact, and the resulting geometries are provided in the Supporting Information. After that, the average oxygen binding energy ($E_{bind,O}$) and the change in surface free energy with respect to Pt(111) ($\Delta\gamma$) for each of the PtO_2 stripes have been calculated. They are compared to the DFT results in Table 1. For most PtO_2 stripes there is very good agreement between the results from DFT and the ReaxFF force field. The 2/3 stripe exhibits by far the worst agreement. It is quite possible that this occurs because the PtO_4-like moiety in this structure is more dissimilar to the platinum oxides used to construct the force field than the more common PtO_2-like stripes.[22] On the other hand, $E_{bind,O}$ and $\Delta\gamma$ show excellent agreement for the 7/8 and 8/9 stripes. This is most important in this context because these two PtO_2 stripes have been identified as most stable under the conditions of the *in situ* STM experiments.

3.2. Spoke Wheel Structure. Guided by the atomistic model tentatively suggested by van Spronsen et al.[15] based on the STM pictures, various candidate structures for the spoke wheel have been considered, including various different

Table 1. Comparison of Energetics for PtO_2 Stripe Structures between ReaxFF[22] and DFT[21] [a]

PtO_2 stripe	$E^{FF}_{bind,O}$ (eV)	$E^{DFT}_{bind,O}$ [21,37] (eV)	$E^{FF\text{-}DFT}_{bind,O}$ (eV)	$\Delta\gamma_{FF}(0)$ (meV Å^{-2})	$\Delta\gamma_{DFT}(0)$ [21,37] (meV Å^{-2})
2/3	−0.37	−0.71	0.34	−38	−69
3/4	−0.76	−0.66	−0.10	−85	−72
4/4	−0.54	−0.51	−0.03	−81	−75
4/5	−0.58	−0.68	0.09	−71	−79
5/6	−0.77	−0.71	−0.06	−96	−87
7/8	−0.74	−0.73	−0.02	−98	−93
8/9	−0.72	−0.72	−0.00	−96	−93

[a] $E_{bind,O}$ is calculated according to eq 7. $\Delta\gamma(0)$ is the change in surface free energy with respect to bare Pt(111) for $\Delta\mu_O = 0$.

supercells of the Pt(111) surface unit cell. Because of the lack of chemical contrast in those experiments, individual (chemisorbed) oxygen adatoms were added at various adsorption sites and (local) coverages between the spokes to the energetically most favorable candidate structures—relying on both chemical intuition based on experimentally observed ordered structures (see Figure 2) and picking random site combinations. The "final" spoke wheel structure shown in Figure 4 is based on an 8 × 8 supercell with 22.3 Å long spokes oriented along the cell vectors. This is in excellent agreement with the spoke length of 22.0(1) Å determined in the STM

https://doi.org/10.1021/acs.jpcc.2c05769
J. Phys. Chem. C 2022, 126, 20020−20027

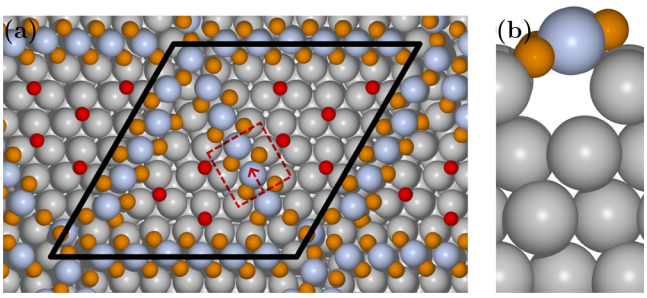

Figure 4. Relaxed structure of the spoke wheel-like platinum surface oxide. Chemisorbed oxygen atoms and ionic oxygen are shown in red and orange, respectively, while metallic and oxidized Pt atoms are indicated in gray and blue, respectively. (a) Top view of the spoke wheel structure, $\theta^{ox} = 0.56$. The unit cell is shown in black and corresponds to a size of 22.3 Å × 22.3 Å. (b) Cross section of the area marked by the red dashed rectangle in the left panel.

experiments.[15] The average Pt−Pt distance within the spokes is 3.10(2) Å, which also matches very well with the experimentally value of 3.10(1) Å. Overall, these spokes are very similar to the PtO_2 stripes; however, they are oriented along the three different high-symmetry directions of the Pt(111) surface. Comparing the geometry of the Pt atoms in the spokes to that of the PtO_2 stripes, as well as previous DFT results for similar structures, it is reasonable to assume that the platinum atoms in these spokes are similarly oxidized (Figure 4b).[38] Therefore, all the Pt atoms that are buckled up by at least 1 Å with respect to the top Pt(111) layer are indicated as oxidized in Figure 4. All oxygen atoms that are coordinated with these Pt atoms ($d_{O-Pt} < 2.5$ Å) are marked in orange. The unbuckled Pt(111) surface between the spokes is covered by chemisorbed oxygen, indicated in red, with a $\sqrt{3} \times \sqrt{3}$-like adsorption geometry.

Figure 5 shows the Gibbs free energy per surface area (γ) of the spoke wheel, the PtO_2 stripes, and several simple adsorption structures of atomic oxygen (see Figure 2) at T = 529 K and p_O = 1 bar. These are the conditions for which the spoke wheel is observed experimentally (corresponding to $\Delta\mu_O(529\text{ K}, 1\text{ bar}) = -0.53$ eV in eq 3). γ values for the 3/4, 5/6, 7/8, and 8/9 PtO_2 stripes and the spoke wheel structures are very similar (within ≈10 meV Å^{-2}). All of these surface oxide structures are considerably more stable than the adsorbed oxygen overlayers. For the PtO_2 stripes, Hanselman et al.[21] have shown that the vibrational contribution can easily exceed 4 meV Å^{-2} according to a reduced-dimensional DFT model. Using the simple Einstein model described in Section 2.1, the influence of vibrational contributions on γ is estimated and shown as error bars in Figure 5. This leads to uncertainties of up to 15 meV Å^{-2}. The surface Gibbs free energies of the spoke wheel structure and the aforementioned four most stable PtO_2 stripes are all within 10 meV Å^{-2} of each other. Consequently, the relative stability of spoke wheel vs stripes could ultimately be determined by the vibrational contribution.

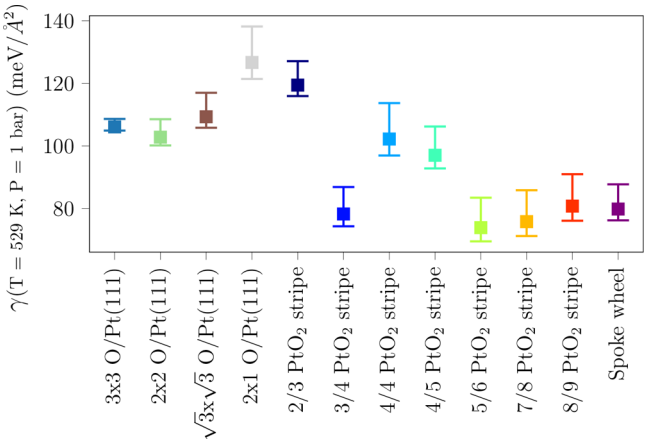

Figure 5. $\gamma(T = 529\text{ K}, p_O = 1\text{ bar})$ for the Pt(111) oxide surface structures shown in Figures 2−4, as calculated using a ReaxFF force field. Error bars indicate the maximal deviations of γ due to the contribution of the vibrational contribution to the Gibbs free energy per surface area, estimated using the Einstein model described in Section 2.1.

In the *in situ* STM experiments,[15] the spoke wheel structures transform into stripe-like structures for an O_2 partial pressure of ≥2.2 bar. This tentatively suggests that the spoke wheel is more stable at smaller values of $\Delta\mu_O$. Figure 6 shows γ of the most relevant structures from Figure 5 over a larger range of $\Delta\mu_O$. Without considering the vibrational free surface energy, the spoke wheel structure is more stable than the PtO_2 stripes at $\Delta\mu_O < -0.7$ eV. This corresponds to temperatures of ≈150 K higher than in the experiment of van Spronsen et al.[15] While the present results do allow to conclude that the spoke wheel structure is the most stable at the experimental conditions after inclusion of the vibrational free surface energy, it seems likely that the vibrational free surface energy will compensate at least partially for the ≈4 meV Å^{-2} difference between the spoke wheel structure and the 7/8 PtO_2 stripe. Because the θ^{ox} of the 7/8 PtO_2 stripe is much higher than the spoke wheel, it seems reasonable that the inclusion of vibrational free energy is in favor of the spoke wheel, as the change in vibrational free

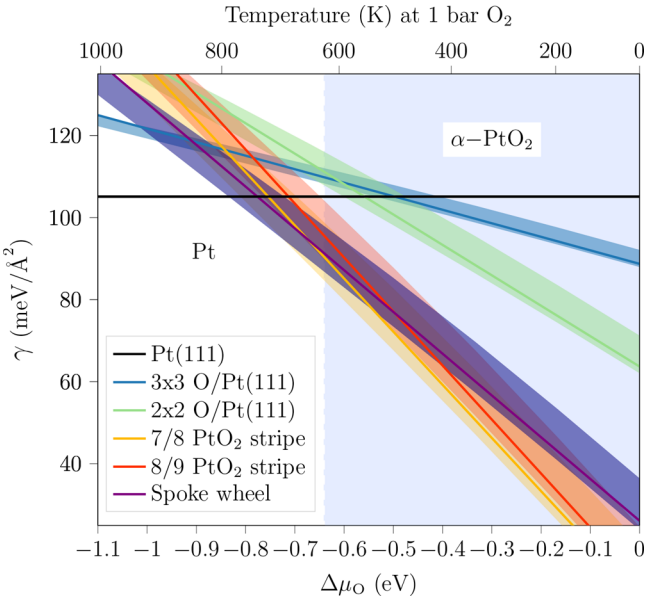

Figure 6. Phase diagram for the Pt(111) surface including various surface structures from Figures 2 to 4 as a function of the oxygen chemical potential $\Delta\mu_O$, calculated using a ReaxFF force field. The most stable bulk phase is indicated by blue and white for α-PtO_2 and fcc-Pt, respectively. Estimations of maximal ($\nu_{O-Pt} = \nu_{O,ads}$) and minimal ($\nu_{O-Pt} = \nu^{(1-3)}_{O-Pt,oxide}$) values of γ for each structure due to vibrational contribution (see Section 2.1) are indicated by shaded regions.

https://doi.org/10.1021/acs.jpcc.2c05769
J. Phys. Chem. C 2022, 126, 20020−20027

energy of oxidic Pt−O bonds under these conditions is more destabilizing ($\Delta F_{vib}^{Pt-O,ox} > 0$), while for adsorbed oxygen it is stabilizing ($\Delta F_{vib}^{Pt-O,ad} < 0$). Finally, as discussed in Section 2, the absolute location of most stable phases on the temperature axis in Figure 6 is very likely affected by the accuracy of the oxygen adsorption energies, whereas this is less relevant for their relative sequence.[36]

3.3. Implications for the Initial Oxidation of Pt(111).

During the experiment of van Spronsen et al.[15] both spoke wheel and stripe-like structures were initially observed simultaneously; however, at higher O_2 pressures the PtO_2 stripes dominate completely. One of the biggest differences between the spoke wheel and PtO_2 stripes is that the surface is oxidized much more in the case of the stripes ($0.67 \leq \theta_{stripes}^{ox} \leq 1.0$ versus $\theta_{spoke\ wheel}^{ox} = 0.56$ as indicated in Figures 3 and 4, respectively). At these experimental conditions, bulk α-PtO_2 is more thermodynamically stable than metallic Pt (see Figure 6). Consequently, the stripe structures are expected to transition into a 2D $PtO_2(0001)$-like film and eventually into a bulk oxide.[38,39] One can thus consider the spoke wheel structure as another metastable platinum surface oxide on the way to forming a (bulk) oxide.

In light of the experimental observations, we assume that kinetic hindrance of elementary steps at the atomic scale underlying the oxide growth make this a rather slow process, which can therefore described by an adiabatic sequence of thermodynamic quasi-equilibria that are established at each oxide coverage θ^{ox}. To examine the stability of the spoke wheel in this context, we have investigated additional structures that could be relevant for $0.0 \leq \theta^{ox} \leq 1.0$. Partially oxidized surfaces with varying θ^{ox} have been created by increasing the space between individual PtO_2 stripes and either leaving it void (i.e, as bare Pt(111)) or filling it up with O/Pt(111) adsorption motifs from Figure 2. This is visualized in Figure 7 together with a naming convention for the resulting structures. As detailed in the Supporting Information, we have determined the most stable structure for each θ^{ox} at T = 529 K and p_{O_2}=1 bar. Figure 8 shows the Gibbs free energy of the most stable partially formed PtO_2 stripe structures at the experimental conditions of the *in situ* STM experiments for intervals of θ^{ox} increasing by 0.1. It is evident that the spoke wheel structure is far more stable than the partially formed PtO_2 stripes with similar θ^{ox}. This suggests that it is simply another metastable surface oxide structure toward the formation of a $PtO_2(0001)$-like film, which could also explain why it is reduced far too rapidly under ultra-high vacuum conditions to be observable *ex situ* in experiments. However, although the sampling of partial oxidation structures is systematic with respect to the employed motifs that have been used as building blocks and can be considered to be accurately described by the Pt−O ReaxFF, it might still not be sufficient to cover the entire relevant phase space.

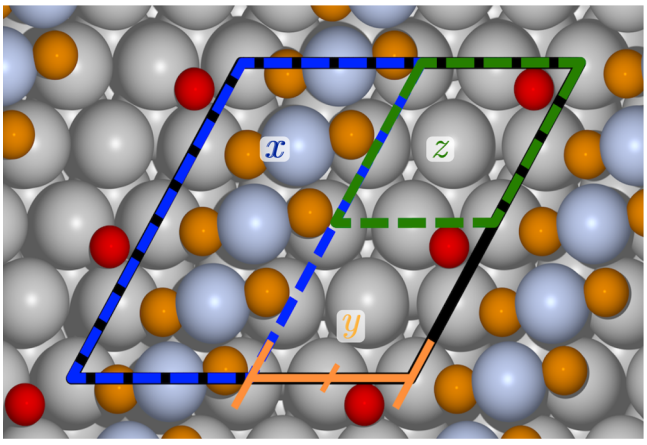

Figure 7. Structures discussed in Figure 8 are named according to the following convention "x + y O/Pt (z)", whereby x indicates the structure of the oxide row, according to the naming scheme of Hanselman et al.[21] (Figure 3), y indicates the number of Pt atoms between adjacent oxide rows, and z indicates the adsorption structure of oxygen on the metallic part of the Pt(111) surface (Figure 2). According to this notation, the structure depicted in this figure is termed "4/4 + 2 O/Pt (2 × 2)".

4. CONCLUSIONS AND OUTLOOK

We have shown that the Pt−O ReaxFF developed by Fantauzzi et al.[22] can reproduce recently published DFT results for PtO_2 stripe structures[21] with good accuracy. Encouraged by this finding and the concomitant possibility to study much larger structures thanks to the considerably lower computational cost, we have used this force field to develop a structural model for the spoke wheel platinum surface oxide observed by van Spronsen et al.[15] According to atomistic thermodynamics, the most stable structure found for the spoke wheels is of similar stability as the most favored PtO_2 stripe structures under the temperature and pressure conditions of the *in situ* STM experiments. Our simple estimates for the vibrational contributions to the Gibbs free energy suggest that these might play an important role for the competition between these structures in the phase diagram. To ultimately determine the thermodynamic stability of the spoke wheels versus the stripe structures in thermodynamic equilibrium, a more accurate interaction potential is required. Considering the surface oxides observed in experiment are likely metastable structures along the reaction path toward further oxidation of the Pt(111) surface toward a $PtO_2(0001)$-like film, we have also investigated potential implications for the initial oxidation of Pt(111). Assuming that the latter can be described by an adiabatic sequence of thermodynamic quasi-equilibria due to significant kinetic hindrance of the relevant elementary steps, we have identified our spoke wheel structure as a prominent structure in an oxide coverage regime between 0.5 and 0.6 (using the full $PtO_2(0001)$-like film as reference).

A sensible next step would be to investigate the initial growth of the spoke wheel and PtO_2-stripe structures at the experimental conditions with a computational approach that can sample the free energy landscape more systematically. This would also allow to quantify the influence of configurational entropy further. Going even further, such calculations can also explicitly account for kinetics. e.g., in the form of adaptive kinetic Monte Carlo simulations,[40] which should be computationally possible with the Pt−O ReaxFF also employed here. In fact, the latter has already been used in grand canonical molecular dynamics simulations for this system,[39,41] which, however, have not reported the formation of a spoke wheel-like structure. It is possible that this is due computational limitations, in particular the size of the simulation cell might not have allowed to accommodate such structures. Alternatively, the spoke wheel structure might only form under a very narrow range of thermodynamic conditions that could not be mimicked in the simulations. In any case, further both

https://doi.org/10.1021/acs.jpcc.2c05769
J. Phys. Chem. C 2022, 126, 20020−20027

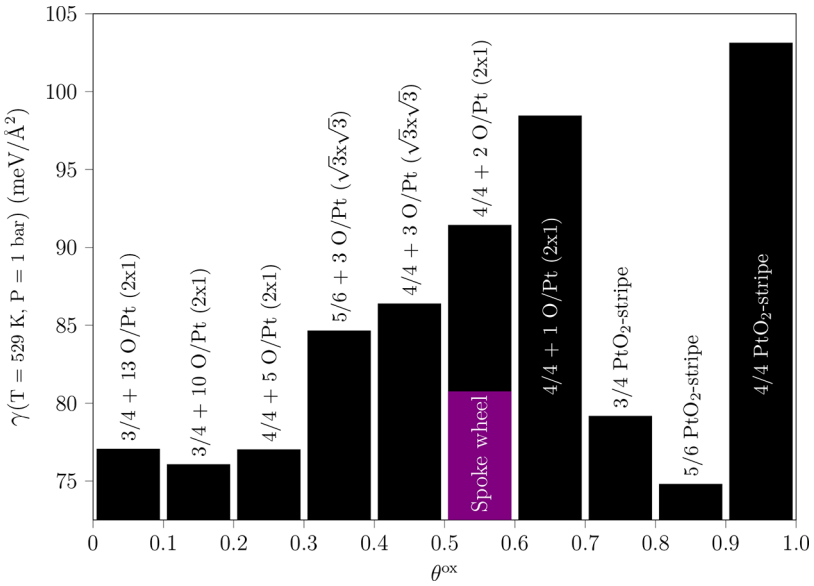

Figure 8. $\gamma(T = 529\ \mathrm{K}, p_O = 1\ \mathrm{bar})$ of the most stable structure for various θ^{ox} from eq 8. The name and γ for the most stable structure in each 0.1 interval is shown. The naming convention used is further explained in Figure 7.

computational and experimental studies are required to better characterize and understand the oxidation of platinum surfaces and thus its state under catalytic conditions.

■ ASSOCIATED CONTENT

Supporting Information

The Supporting Information is available free of charge at https://pubs.acs.org/doi/10.1021/acs.jpcc.2c05769.

Vibrational frequencies with the Pt−O ReaxFF, most stable partially oxidized PtO_2-stripe structures (PDF)

Spoke wheel and PtO_2-stripe structures as optimized with the Pt−O ReaxFF (ZIP)

All partially oxidized PtO_2-stripe structures as optimized with the Pt−O ReaxFF (ZIP)

■ AUTHOR INFORMATION

Corresponding Authors

Dajo Boden − *Leiden Institute of Chemistry, Leiden University, 2300 RA Leiden, The Netherlands*; Email: d.boden@lic.leidenuniv.nl

Jörg Meyer − *Leiden Institute of Chemistry, Leiden University, 2300 RA Leiden, The Netherlands*; orcid.org/0000-0003-0146-730X; Email: j.meyer@chem.leidenuniv.nl

Author

Irene M. N. Groot − *Leiden Institute of Chemistry, Leiden University, 2300 RA Leiden, The Netherlands*; orcid.org/0000-0001-9747-3522

Complete contact information is available at: https://pubs.acs.org/10.1021/acs.jpcc.2c05769

Notes

The authors declare no competing financial interest.

■ ACKNOWLEDGMENTS

The authors thank S. Hanselman for providing "raw" data from his DFT calculations for the PtO_2 stripes (private communications of relaxed geometries and corresponding VASP output files). J. van der Kleij, L. van der Boon, and K. Arts are acknowledged for their contributions to the benchmarking of the Pt−O ReaxFF and development of trial structures for the spoke wheel. The authors are grateful for financial support from the Leiden Institute of Chemistry (LIC).

■ REFERENCES

(1) Koltsakis, G. C.; Stamatelos, A. M. Catalytic automotive exhaust aftertreatment. *Prog. Energy Combust. Sci.* **1997**, *23*, 1−39.

(2) Takahashi, N.; Shinjoh, H.; Iijima, T.; Suzuki, T.; Yamazaki, K.; Yokota, K.; Suzuki, H.; Miyoshi, N.; ichi Matsumoto, S.; Tanizawa, T.; et al. The new concept 3-way catalyst for automotive lean-burn engine: NOx storage and reduction catalyst. *Catal. Today* **1996**, *27*, 63−69.

(3) Ruge, M.; Drnec, J.; Rahn, B.; Reikowski, F.; Harrington, D. A.; Carlà, F.; Felici, R.; Stettner, J.; Magnussen, O. M. Structural Reorganization of Pt(111) Electrodes by Electrochemical Oxidation and Reduction. *J. Am. Chem. Soc.* **2017**, *139*, 4532−4539.

(4) Peng, J.; Tao, P.; Song, C.; Shang, W.; Deng, T.; Wu, J. Structural evolution of Pt-based oxygen reduction reaction electrocatalysts. *Chin. J. Catal.* **2022**, *43*, 47−58.

(5) Tanaka, H.; Nagahara, Y.; Sugawara, S.; Shinohara, K.; Nakamura, M.; Hoshi, N. The Influence of Pt Oxide Film on the Activity for the Oxygen Reduction Reaction on Pt Single Crystal Electrodes. *Electrocatalysis* **2014**, *5*, 354−360.

(6) Langmuir, I. The Adsorption Of Gases On Plane Surfaces Of Glass, Mica And Platinum. *J. Am. Chem. Soc.* **1918**, *40*, 1361−1403.

(7) Hollander, J. M.; Jolly, W. L. X-ray photoelectron spectroscopy. *Acc. Chem. Res.* **1970**, *3*, 193−200.

(8) Jona, F.; Strozier, J. A.; Yang, W. S. Low-energy electron diffraction for surface structure analysis. *Rep. Prog. Phys.* **1982**, *45*, 527−585.

(9) Chang, C. C. Auger electron spectroscopy. *Surf. Sci.* **1971**, *25*, 53−79.

(10) Goodman, D. W. Model Studies in Catalysis Using Surface Science Probes. *Chem. Rev.* **1995**, *95*, 523−536.

(11) Nørskov, J. K.; Abild-Pedersen, F.; Studt, F.; Bligaard, T. Density functional theory in surface chemistry and catalysis. *Proc. Natl. Acad. Sci. U. S. A.* **2011**, *108*, 937−943.

(12) Wang, Z.; Hu, P. Towards rational catalyst design: a general optimization framework. *Philos. Trans. R. Soc. A* **2016**, *374*, 20150078.

(13) Zhang, S.; Nguyen, L.; Zhu, Y.; Zhan, S.; Tsung, C.-K. F.; Tao, F. F. In-Situ Studies of Nanocatalysis. *Acc. Chem. Res.* **2013**, *46*, 1731−1739.

(14) Tao, F. F.; Crozier, P. A. Atomic-Scale Observations of Catalyst Structures under Reaction Conditions and during Catalysis. *Chem. Rev.* **2016**, *116*, 3487−3539.
(15) van Spronsen, M. A.; Frenken, J. W. M.; Groot, I. M. N. Observing the oxidation of platinum. *Nat. Commun.* **2017**, *8*, 2041−1723.
(16) Reuter, K.; Scheffler, M. First-Principles Atomistic Thermodynamics for Oxidation Catalysis: Surface Phase Diagrams and Catalytically Interesting Regions. *Phys. Rev. Lett.* **2003**, *90*, 046103.
(17) Nørskov, J. K.; Scheffler, M.; Toulhoat, H. Density Functional Theory in Surface Science and Heterogeneous Catalysis. *MRS Bull.* **2006**, *31*, 669−674.
(18) Rogal, J.; Reuter, K.*Ab Initio Atomistic Thermodynamics for Surfaces: A Primer*, 2007.
(19) Sutton, C.; Levchenko, S. V. First-Principles Atomistic Thermodynamics and Configurational Entropy. *Front. Chem.* **2020**, *8*, 757.
(20) Sun, Q.; Reuter, K.; Scheffler, M. Effect of a humid environment on the surface structure of RuO_2(110). *Phys. Rev. B* **2003**, *67*, 205424.
(21) Hanselman, S.; McCrum, I. T.; Rost, M. J.; Koper, M. T. M. Thermodynamics of the formation of surface PtO_2 stripes on Pt(111) in the absence of subsurface oxygen. *Phys. Chem. Chem. Phys.* **2020**, *22*, 10634−10640.
(22) Fantauzzi, D.; Bandlow, J.; Sabo, L.; Mueller, J. E.; van Duin, A. C. T.; Jacob, T. Development of a ReaxFF potential for Pt−O systems describing the energetics and dynamics of Pt-oxide formation. *Phys. Chem. Chem. Phys.* **2014**, *16*, 23118−23133.
(23) van Duin, A. C. T.; Dasgupta, S.; Lorant, F.; Goddard, W. A. ReaxFF: A Reactive Force Field for Hydrocarbons. *J. Phys. Chem. A* **2001**, *105*, 9396−9409.
(24) van Duin, A. C. T.; Strachan, A.; Stewman, S.; Zhang, Q.; Xu, X.; Goddard, W. A. ReaxFFSiO Reactive Force Field for Silicon and Silicon Oxide Systems. *J. Phys. Chem. A* **2003**, *107*, 3803−3811.
(25) Keith, J. A.; Fantauzzi, D.; Jacob, T.; van Duin, A. C. T. Reactive forcefield for simulating gold surfaces and nanoparticles. *Phys. Rev. B* **2010**, *81*, 235404.
(26) Reuter, K.; Scheffler, M. Composition, structure, and stability of RuO_2(110) as a function of oxygen pressure. *Phys. Rev. B* **2001**, *65*, 035406.
(27) Stull, D. R.; Prophet, H.*JANAF Thermochemical Tables*, 2nd ed.; U.S. Dept. of Commerce, National Bureau of Standards: Washington, DC, 1971.
(28) Abraham, F. F.; Dave, J. V. On a Generalized Einstein Theory for the Thermodynamics of Planar Surfaces and Microcrystallites. *J. Chem. Phys.* **1971**, *55*, 4817−4821.
(29) Peuckert, M.; Ibach, H. Vibrational spectra of an oxidized platinum electrode. *Surf. Sci.* **1984**, *136*, 319−326.
(30) Aktulga, H.; Fogarty, J.; Pandit, S.; Grama, A. Parallel reactive molecular dynamics: Numerical methods and algorithmic techniques. *Parallel Comput* **2012**, *38*, 245−259.
(31) Chenoweth, K.; van Duin, A. C. T.; Goddard, W. A. ReaxFF Reactive Force Field for Molecular Dynamics Simulations of Hydrocarbon Oxidation. *J. Phys. Chem. A* **2008**, *112*, 1040−1053.
(32) Thompson, A. P.; Aktulga, H. M.; Berger, R.; Bolintineanu, D. S.; Brown, W. M.; Crozier, P. S.; in 't Veld, P. J.; Kohlmeyer, A.; Moore, S. G.; Nguyen, T. D.; et al. LAMMPS - a flexible simulation tool for particle-based materials modeling at the atomic, meso, and continuum scales. *Comput. Phys. Commun.* **2022**, *271*, 108171.
(33) Larsen, A. H.; Mortensen, J. J.; Blomqvist, J.; Castelli, I. E.; Christensen, R.; Dułak, M.; Friis, J.; Groves, M. N.; Hammer, B.; Hargus, C.; et al. The Atomic Simulation Environment—a Python Library for Working with Atoms. *J. Phys.: Condens. Matter* **2017**, *29*, 273002.
(34) Perdew, J. P.; Burke, K.; Ernzerhof, M. Generalized Gradient Approximation Made Simple. *Phys. Rev. Lett.* **1996**, *77*, 3865−3868.
(35) Zhang, Y.; Yang, W. Comment on "Generalized Gradient Approximation Made Simple. *Phys. Rev. Lett.* **1998**, *80*, 890.
(36) Rogal, J.; Reuter, K.; Scheffler, M. CO oxidation at Pd(100): A first-principles constrained thermodynamics study. *Phys. Rev. B* **2007**, *75*, 205433.
(37) We note that $E_{\mathrm{bind,O}}^{\mathrm{DFT}}$ has not been explicitly evaluated in ref 21. Nevertheless, the required total energies from the DFT calculations with the VASP code are available in the accompanying Supporting Information for that work.
(38) Hawkins, J. M.; Weaver, J. F.; Asthagiri, A. Density functional theory study of the initial oxidation of the Pt(111) surface. *Phys. Rev. B* **2009**, *79*, 125434.
(39) Fantauzzi, D.; Krick-Calderón, S.; Mueller, J. E.; Grabau, M.; Papp, C.; Steinrück, H.-P.; Senftle, T. P.; van Duin, A. C. T.; Jacob, T. Growth of Stable Surface Oxides on Pt(111) at Near-Ambient Pressures. *Angew. Chem., Int. Ed.* **2017**, *56*, 2594−2598.
(40) Henkelman, G.; Jónsson, H. Long time scale kinetic Monte Carlo simulations without lattice approximation and predefined event table. *J. Chem. Phys.* **2001**, *115*, 9657−9666.
(41) Jung, C. K.; Braunwarth, L.; Jacob, T. Grand Canonical ReaxFF Molecular Dynamics Simulations for Catalytic Reactions. *J. Chem. Theory Comput.* **2019**, *15*, 5810−5816.

https://doi.org/10.1021/acs.jpcc.2c05769
J. Phys. Chem. C 2022, 126, 20020−20027